Asociación Argentina
de Mecánica Computacional

Mecánica Computacional Vol XXIX, págs. 5705-5727 (artículo completo)
Eduardo Dvorkin, Marcela Goldschmit, Mario Storti (Eds.)
Buenos Aires, Argentina, 15-18 Noviembre 2010

A SUPERCONVERGENT TEMPERATURE PATCH PROCEDURE FOR NODAL FLUX RECOVERY IN FINITE ELEMENT COMPUTATIONS

Pablo A. Muñoz-Rojas, Marcos F. Odorczyk, Eduardo L. Cardoso and Miguel Vaz Jr.

Departamento de Engenharia Mecânica, Universidade do Estado de Santa Catarina, Campus Universitário Avelino Marcante, s/n, Bom Retiro, 89223-100, Joinville, SC, Brasil

Keywords: Flux revovery procedures, Finite Element Method, Heat transfer.

Abstract. This article shows a new procedure for the evaluation of nodal flux fields in heat transfer analyses. Although, in principle, the idea can be easily adapted to discretization procedures other than the Finite Element Method (FEM), the numerical properties observed herein cannot be taken as universal. In the FEM framework, the proposed method shows a behavior similar to the SPR method introduced by Zhu and Zienkiewicz, especially with respect to low mesh distortion sensitivity and high convergence rate. As an advantage, the present method is computationally more efficient. The method can also be applied to elasticity or thermoelasticity problems in order to recover stresses, in which case the enhanced efficiency is even more significant. The qualitative behavior of the proposed technique is discussed using 2D conduction problems with prescribed temperature and flux boundary conditions.

1 INTRODUCTION

Derivative-based quantities in most finite element approximations present a discontinuous field at the element interfaces. To overcome this inconvenient, many strategies have been proposed over the last decades: averaged simple nodal evaluation, averaged extrapolation using a reduced polynomial (Barlow, 1976), local and global, continuous and discrete smoothing procedures (Hinton and Campbell, 1974) and recovery based on patches - SPR (Zienkiewicz and Zhu, 1992; Boroomand and Zienkiewicz, 1997), among others.

This work presents a recovery method based on patches of nodal temperature so that computation of nodal heat flux is based upon the corresponding patch field derivatives combined with material properties evaluated directly at the nodal points. Such technique would avoid extrapolation errors when nonhomogeneous material properties are used.

This method presents improved computational efficiency due to a reduction on the number of linear systems to be solved and similar accuracy with respect to existing superconvergent methods, such as the classical SPR. The proposed heat flux recovery strategy presents excellent results regarding global convergence rate, mesh distortion and fluxes computed at boundary nodes. Both classical and proposed patch recovery techniques yield better results than strategies based on direct nodal computation, smoothing and extrapolation methods.

2 MATHEMATICAL MODEL AND DISCRETIZATION

Starting from the energy conservation law and the Fourier heat conduction equation, the 2D steady state heat conduction problem in homogeneous isotropic media can be modeled by the differential equation

$$k\left(\frac{\partial^2 T}{\partial x^2}+\frac{\partial^2 T}{\partial y^2}\right)+Q=0 \tag{1}$$

where Q is the rate of heat generation per unit volume, k is the thermal conductivity and T is the temperature. Temperature or flux boundary conditions can be appropriately imposed on parts of the boundary. In homogeneous isotropic media, flux in direction $\boldsymbol{\nu}$ is given by

$$q_\nu = -q_B = -k\frac{\partial T}{\partial \nu} \tag{2}$$

where

$$\frac{\partial T}{\partial \nu}=\frac{\partial T}{\partial x}l+\frac{\partial T}{\partial y}m \tag{3}$$

and l and m are the direction cosines of $\boldsymbol{\nu}$, as depicted in Fig. 1.

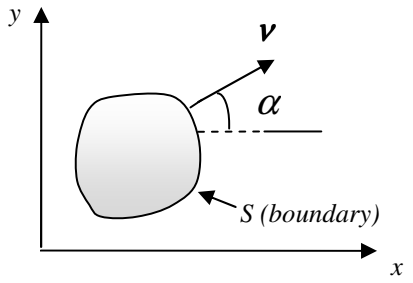

Figure 1. Outward surface-normal unit vector.

Equilibrium given by Eq.(1) can be alternatively found by the minimization of the associate functional

$$\Pi = \int \left(\frac{1}{2} \begin{Bmatrix} T_{,x} \\ T_{,y} \end{Bmatrix} k \begin{Bmatrix} T_{,x} & T_{,y} \end{Bmatrix} - QT \right) dV - \int q_B T dS \tag{4}$$

where $(\cdot)_{,x} = \partial(\cdot)/\partial x$ and $(\cdot)_{,y} = \partial(\cdot)/\partial y$.

2.1 Finite element formulation

The temperature field can be expressed by an approximation in terms of element nodal temperatures $\{T_e\}$ by

$$T = [N]\{T_e\} \tag{5}$$

where $[N]$ is the interpolation functions matrix. Similarly, the temperature gradient vector can be expressed as

$$\{T_\partial\} = [B]\{T_e\} \tag{6}$$

where

$$\{T_\partial\} = \begin{Bmatrix} T,_x \\ T,_y \end{Bmatrix}, \qquad [B] = \{\partial\}[N] \qquad \text{and} \qquad \{\partial\} = \begin{Bmatrix} \partial/\partial x \\ \partial/\partial y \end{Bmatrix} \tag{7-9}$$

By replacing Eq.(6) in the functional given by Eq.(4), one gets

$$\Pi^* = \int \left(\frac{1}{2} \{T_\partial\}^T k \{T_\partial\} - QT \right) dV - \int q_B T dS \tag{10}$$

or

$$\Pi^* = \frac{1}{2} \{T_e\}^T [\mathbf{k}] \{T_e\} - \{T_e\}^T \left(\{r_B\} + \{r_Q\} \right) \tag{11}$$

from which minimization provides the discretized element equilibrium equations

$$[\mathbf{k}]\{T_e\} = \{R_e\} \tag{12}$$

where

$$[\mathbf{k}] = \int_V [B]^T k [B] \tau \, dV \tag{13}$$

$$\{R_e\} = \{r_B\} + \{r_Q\} \tag{14}$$

$$\{r_B\} = \int_S [B]^T q_B dS \quad \text{and} \quad \{r_Q\} = \int_V [B]^T Q dV \tag{15-16}$$

In order to obtain the equilibrium equations for the whole domain, element contributions must be added, yielding the assembled global discretized equilibrium equations

$$[\mathbf{K}]\{T\} = \{R\} \tag{17}$$

3 HEAT FLUX RECOVERY PROCEDURES

3.1 Introduction

Accurate nodal heat flux determination in finite elements is an issue of major concern in engineering practice. Thermal analysis often requires computation, not only of the temperature field, but also heat transfer characteristics. Examples of such situations are the simulation of heat treatment of materials, welding processes and machining operations amongst others.

In finite element computations heat flux values can be shown to be poor at the nodes and most accurate inside the elements, specifically at the so-called Barlow points (Barlow,1976). In order to obtain high quality nodal flux values, different post-processing schemes have been proposed. The conception of such schemes is identical to procedures developed for nodal stress recovery in elasticity (the problems are analogous since both, fluxes and stresses are evaluated by differentiation of the primal field – temperature and displacements). In this Section some traditional nodal flux recovery procedures are briefly described and later used for comparison purposes. Details on the recovery strategy introduced in this work are presented in Section 4.

Figure 2 presents typical 4 and 9 node elements emphasizing the position of their nodes and Gauss integration points (Wildemann and Muñoz-Rojas, 2005). These positions are mentioned throughout the text, since all the post-processing schemes studied evaluate fluxes on them.

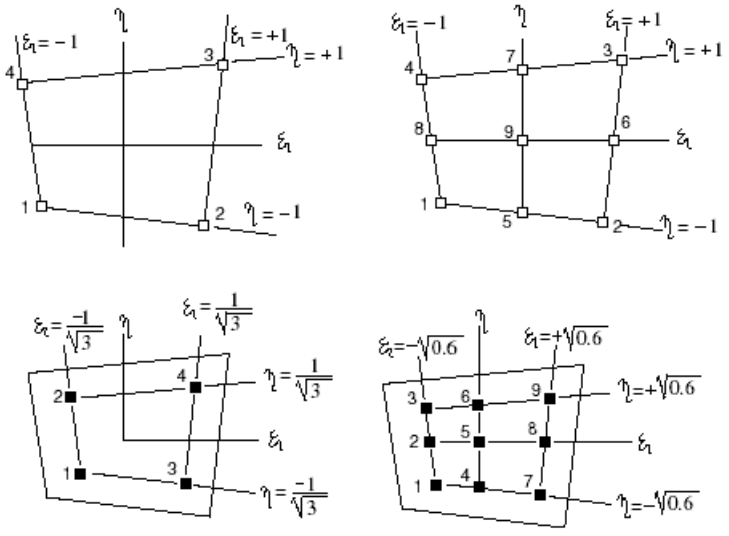

Figure 2. Parametric coordinates of the nodes and Gauss integration points for 4 and 9 node elements.

3.2 Heat flux evaluation directly on the nodes

Once the temperature field is determined via the solution of Eq.(17), the flux fields can be obtained using the discretized version of the Fourier law in each element,

$$\{\hat{\boldsymbol{q}}\} = -k[\boldsymbol{B}]\{\boldsymbol{T}_e\} \tag{18}$$

Since global interpolation functions have only C_0 continuity in temperature based finite elements, flux jumps occur in the interfaces between elements. Thus, when one node is shared by several surrounding elements, nodal flux values given by Eq.(18) provide different results

when calculated with reference to each of the elements. A common procedure in this case is to approximate the nodal result by the corresponding mean value. This method generally yields poor result because flux errors are normally large on the element edges.

3.3 Extrapolation using a reduced order polynomial

It can be shown that Barlow points are very close to Gauss integration points associated to reduced order polynomials. If the exact integration of Eq.(13) (in an undistorted mesh) requires *n* points in each direction, reduced integration is given by *n-1* points in the associated Gauss locations. Flux values can be evaluated in these points and extrapolated to the nodes using the associated reduced order interpolation functions (Cook et al, 2001). This scheme usually renders improved results when compared to heat flux evaluation directly at the nodes.

3.4 Global L_2 smoothing

This strategy assumes a global heat flux field continuous on the whole domain, including element interfaces. The field is interpolated within an element using the interpolation functions $[\boldsymbol{N}]$:

$$\{\boldsymbol{q}(\xi,\eta)\} = [\boldsymbol{N}]\left\{\bar{\boldsymbol{q}}\right\} \tag{19}$$

where $\left\{\bar{\boldsymbol{q}}\right\}$ are the smoothed nodal flux values.

The difference between the smoothed and the *raw* (discontinuous) flux fields is given by

$$\{\boldsymbol{\varphi}(\xi,\eta)\} = \{\boldsymbol{q}(\xi,\eta)\} - \{\hat{\boldsymbol{q}}(\xi,\eta)\} \tag{20}$$

where $\{\hat{\boldsymbol{q}}\}$ is the *raw* flux field.

Minimization of the squared difference given in Eq.(20) with respect to $\{\hat{\boldsymbol{q}}\}$ provides the closest projection of the continuous field to the discontinuous one. The function to be minimized is

$$J_1 = \frac{1}{2}\int_{\Omega} [\boldsymbol{\varphi}(\xi,\eta)]^T [\boldsymbol{\varphi}(\xi,\eta)] J d\xi d\eta \tag{21}$$

whose minimization yields

$$\int\int [\boldsymbol{N}]^T(\xi,\eta)\boldsymbol{\varphi}(\xi,\eta) J d\xi d\eta \;\; = \boldsymbol{0} \tag{22}$$

After some manipulation, Eq. (22) can be written as

$$\left[\int\int [\boldsymbol{N}]^T [\boldsymbol{N}] J\, d\xi\, d\eta\right]\{\boldsymbol{q}\} = \left\{\int\int [\boldsymbol{N}]^T k [\boldsymbol{B}] J\, d\xi\, d\eta \{\boldsymbol{T}_e\}\right\} \tag{23}$$

where

$$[\boldsymbol{M}] = \int\int [\boldsymbol{N}]^T [\boldsymbol{N}] J\, d\xi\, d\eta \tag{24}$$

is the global mass matrix and

$$[\boldsymbol{P}] = \int\int [\boldsymbol{N}]^T k\, [\boldsymbol{B}] J d\xi d\eta \{\boldsymbol{T}_e\} \tag{25}$$

is the pseudo-load vector. Equation (25) can be written as

$$\begin{bmatrix} [\boldsymbol{M}] & [\boldsymbol{0}] \\ [\boldsymbol{0}] & [\boldsymbol{M}] \end{bmatrix} \begin{Bmatrix} \bar{\boldsymbol{q}}_x \\ \bar{\boldsymbol{q}}_y \end{Bmatrix} = \begin{Bmatrix} \{\boldsymbol{P}_1\} \\ \{\boldsymbol{P}_2\} \end{Bmatrix} \tag{26}$$

which is a *block uncoupled* system and can be solved more efficiently as represented below.

$$[\boldsymbol{M}] \left[\left\{ \bar{\boldsymbol{q}}_x \right\} \quad \left\{ \bar{\boldsymbol{q}}_y \right\} \right] = \left[\{\boldsymbol{P}_1\} \quad \{\boldsymbol{P}_2\} \right] \tag{27}$$

The computational effort associated to this method is high; it can be noticed that the order of the linear system in Eq.(27) is equal to the number of nodes in the discretization (an iterative alternative has been presented in Wildemann e Muñoz-Rojas, 2005). In spite of this inconvenient, the procedure has the advantage of providing continuous flux results through the whole domain.

3.5 Element based superconvergent patch recovery (SPR)

In the reduced order polynomial strategy described in Section 3.3, high quality flux values sampled at corresponding reduced order Gauss locations are used for extrapolation purposes. Due to the low quantity of information, extrapolation to the nodes must be done using reduced order interpolation functions. If additional high quality flux values could be found and sampled, it would be possible to use higher order polynomials for extrapolation to the nodes, thus increasing accuracy. The idea can be implemented by defining a patch of elements surrounding either a particular node or a particular element, as shown in Fig. 3.

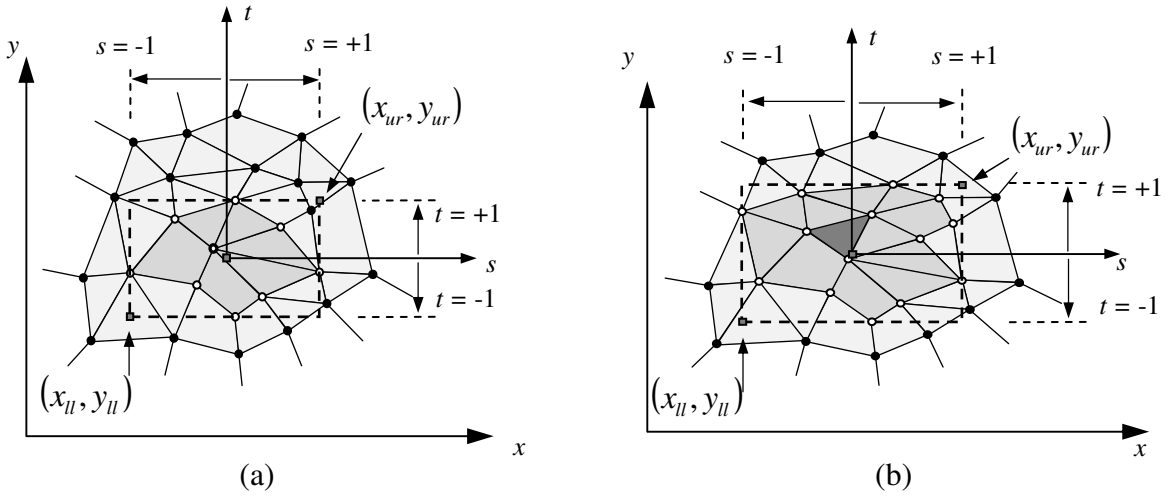

Figure 3. Examples of element patches: (a) centered on nodes; (b) centered on elements.

Fluxes are sampled at the reduced integration points of all the elements in the patch, and an approximate flux surface valid on the patch can be adjusted using higher order polynomials. The smooth field obtained on the patch is represented by

$$q_i^* = [\boldsymbol{P}] \{\boldsymbol{a}\} \tag{28}$$

where q_i^* stands for each of the flux vector components, $[\boldsymbol{P}]$ contains polynomial terms and $\{\boldsymbol{a}\}$ contains generalized coordinates to be determined.

In order to determine $\{\boldsymbol{a}\}$ and find the smoothed flux fields, it is convenient to define a local reference system with coordinates ranging in the interval [-1,+1], which helps to avoid possible ill-conditioning difficulties. In this work the patches are centered in elements and, following Akin (2005), the local reference system was defined parallel to the global system but centered on a rectangular superelement, which contains the patch, as illustrated in Fig. 3.

The global coordinates are related to the local ones (patch superelement) by

$$s = -1 + \frac{2}{x_{ur} - x_{ll}}\left(x - x_{ll}\right) \quad \text{and} \quad t = -1 + \frac{2}{y_{ur} - y_{ll}}\left(y - y_{ll}\right) \tag{29}$$

where (x_{ll}, y_{ll}) and (x_{ur}, y_{ur}) are the coordinates of the lower left and upper right corners of the superelement, respectively, as shown in Fig. 3.

In a plane problems, some possibilities for the polynomial matrix are

Linear using 3 terms (SPRE): $\lfloor \boldsymbol{P} \rfloor = \lfloor 1 \quad s \quad t \rfloor$ (30)

Linear using 4 terms (SPRE4): $\lfloor \boldsymbol{P} \rfloor = \lfloor 1 \quad s \quad t \quad st \rfloor$ (31)

Quadratic using 6 terms (SPRE6): $\lfloor \boldsymbol{P} \rfloor = \lfloor 1 \quad s \quad t \quad st \quad s^2 \quad t^2 \rfloor$ (32)

Quadratic using 8 terms (SPRE8): $\lfloor \boldsymbol{P} \rfloor = \lfloor 1 \quad s \quad t \quad st \quad s^2 \quad t^2 \quad s^2 t \quad st^2 \rfloor$ (33)

Quadratic using 9 terms (SPRE9): $\lfloor \boldsymbol{P} \rfloor = \lfloor 1 \quad s \quad t \quad st \quad s^2 \quad t^2 \quad s^2 t \quad st^2 \quad s^2 t^2 \rfloor$ (34)

Flux values are sampled at the reduced polynomial locations within each finite element belonging to the patch. At each *j-th* sampling point $\left(x_j, y_j\right)$, the squared difference between the flux q_i and the still unknown q_i^* is evaluated. The squared terms are added, yielding

$$J_2 = \frac{1}{2}\sum_{j=1}^{nsp}\left(q_i^* - q_i\right)_j^2 \tag{35}$$

where *nsp* is the number of sampling points in the patch. The minimization of Eq.(35) with respect to $\{\boldsymbol{a}\}$ results in

$$[\boldsymbol{A}]\{\boldsymbol{a}\} = \{\boldsymbol{b}\} \tag{36}$$

where

$$[\boldsymbol{A}] = \sum_{j=1}^{nsp}\lfloor \boldsymbol{P} \rfloor_j^T \lfloor \boldsymbol{P} \rfloor_j \tag{37}$$

$$\{\boldsymbol{b}\} = \sum_{j=1}^{nsp}\lfloor \boldsymbol{P} \rfloor_j^T \left(q_i\right)_j \tag{38}$$

Vector $\{\boldsymbol{a}\}$ is determined by the solution of Eq.(36), so that the fluxes can be evaluated everywhere in the patch, including nodal locations, by application of Eq.(28). Noting that each finite element in the domain mesh has its own surrounding patch, the nodes will accumulate different flux values. The final result is given by a simple average.

4 FLUX RECOVERY BASED ON TEMPERATURE PATCHES

The flux recovery strategy presented herein is a modification on the concept of the

superconvergent patch recovery (SPR) detailed in Section 3.5. In this case, a patch is used to generate a polynomial surface to approximate locally the temperature field, rather than the fluxes. Now the nodes are taken as sampling points, and the smoothed temperature field inside the patch is given by

$$T = [\boldsymbol{P}]\{\boldsymbol{a}\}, \tag{39}$$

The procedure leads to the linear system

$$[\boldsymbol{A}]\{\boldsymbol{a}\} = \{\boldsymbol{b}\} \tag{40}$$

where

$$[\boldsymbol{A}] = \sum_{j=1}^{nsp} \lfloor \boldsymbol{P} \rfloor_j^T \lfloor \boldsymbol{P} \rfloor_j \tag{41}$$

$$\{\boldsymbol{b}\} = \sum_{j=1}^{nsp} \lfloor \boldsymbol{P} \rfloor_j^T (T)_j \tag{42}$$

and the fluxes can be obtained by differentiation of Eq.(39),

$$q_x = -k \frac{dT}{dx} \qquad\qquad q_y = -k \frac{dT}{dy} \tag{43-44}$$

where

$$\begin{Bmatrix} \dfrac{dT}{dx} \\ \dfrac{dT}{dx} \end{Bmatrix} = \begin{bmatrix} \dfrac{d\lfloor \boldsymbol{P} \rfloor}{dx} \\ \dfrac{d\lfloor \boldsymbol{P} \rfloor}{dy} \end{bmatrix} \{\boldsymbol{a}\} = \begin{bmatrix} \dfrac{ds}{dx} & \dfrac{dt}{dx} \\ \dfrac{ds}{dy} & \dfrac{dt}{dy} \end{bmatrix} \begin{bmatrix} \dfrac{d\lfloor \boldsymbol{P} \rfloor}{ds} \\ \dfrac{d\lfloor \boldsymbol{P} \rfloor}{dt} \end{bmatrix} \{\boldsymbol{a}\} \tag{45}$$

Note that the derivatives in the Jacobian matrix in Eq.(45) can be obtained by differentiation of Eq.(29). As in the SPR procedure, different flux values will result for each node, depending on the patch considered. The result is given by simple average.

It is worth remarking that this method has an important efficiency gain with respect to the SPR approach. While in the former the solution of Eq.(36) must be performed for each flux component, in the present case a similar linear problem must be solved only for the temperature field. This advantage increases for 3D problems and in applications to stress fields in elasticity problems. Although in small scale problems the difference might not be so relevant, application of this strategy to optimization problems, in which hundreds of evaluations might be necessary, can improve the overall efficiency significantly.

In order to have a procedure able to approximate the flux fields consistently with the SPR approach (so that both methods can be compared), we always adopt a matrix $[\boldsymbol{P}]$ containing polynomials one degree higher than the ones considered in the former. After differentiation present in Eqs.(43-44) the fluxes are represented by polynomials of equal order.

In addition to the quadratic polynomials, considered in the SPR approach (to be applied in the case of linear finite elements), the following cubic polynomials have been studied (applied in the case of quadratic finite elements):

Cubic using 13 terms (PT13):

$$[\boldsymbol{P}]=\begin{bmatrix}1 & s & t & s^2 & st & t^2 & s^2t & ts^2 & s^2t^2 & s^3 & s^3t & st^3 & t^3\end{bmatrix} \tag{46}$$

Cubic using 15 terms (PT15):

$$[\boldsymbol{P}]=\begin{bmatrix}1 & s & t & s^2 & st & t^2 & s^2t & st^2 & s^2t^2 & s^3 & s^3t & st^3 & t^3 & s^3t^2 & s^2t^3\end{bmatrix} \tag{47}$$

Cubic using 16 terms (PT16):

$$[\boldsymbol{P}]=\begin{bmatrix}1 & s & t & s^2 & st & t^2 & s^2t & st^2 & s^2t^2 & s^3 & s^3t & st^3 & t^3 & s^3t^2 & s^2t^3 & s^3t^3\end{bmatrix} \tag{48}$$

5 NUMERICAL EXAMPLES

Three examples were selected in order to show some characteristics of the proposed flux recovery scheme (patch on temperature field - PT). The first test case aims to verify the sensitivity to mesh distortion at a selected node, the second example analyzes the convergence rate in a smooth problem and the third one assesses the heat flux on the boundary. In all the cases, the results are compared with those provided by the additional methods discussed in Section 3. Aiming at a concise notation, these methods are referenced as: D - Direct evaluation at nodes, E – Extrapolation, S – Global smoothing, and SPR – Superconvergent patch recovery.

5.1 Flux sensitivity to mesh distortion

In order to analyze the influence of mesh distortion on the accuracy of different flux post-processing methods, including the temperature patch strategy described in Section 4, a classical heat transfer problem with known analytical solution was studied (Kreith and Bohn, 2010). The problem consists of a rectangular 2D domain, with prescribed temperature boundary conditions on the edges. Figure 4 depicts the geometry, where the length and the height are L = 3m and W = 1m, respectively. Thermal conductivity is given by k = 1.0 W/mK and the prescribed temperatures are T1 = 0 ^{o}C and T2 = 1 ^{o}C.

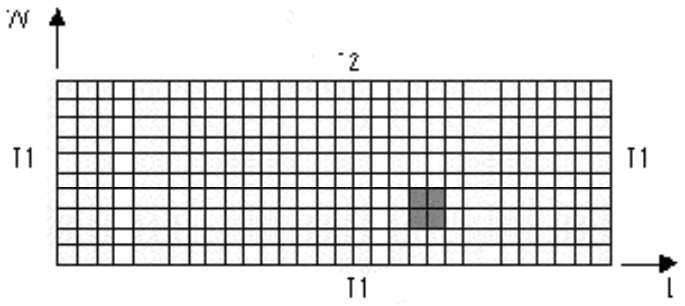

Figure 4. Beam subjected to Temperature field

The analytical solutions for temperature and fluxes are given by

$$T(x,y)=\frac{2}{\pi}\sum_{i=1}^{\infty}\frac{(-1)^{i+1}+1}{i}\sin\left(\frac{i\pi x}{L}\right)\frac{\sinh\left(i\pi y/L\right)}{\sinh\left(i\pi w/L\right)} \tag{49}$$

$$q(x,y)_x = -k\ \frac{2}{L}\sum_{i=1}^{n}\left(\frac{((-1)^{(i+1)}+1)\cos(\frac{i\pi x}{L})\sinh(\frac{i\pi y}{L})}{\sinh(\frac{i\pi w}{L})}\right) \tag{50}$$

$$q(x,y)_y = -k\ \frac{2}{L}\sum_{i=1}^{n}\left(\frac{((-1)^{(i+1)}+1)\sin(\frac{i\pi x}{L})\cosh(\frac{i\pi y}{L})}{\sinh(\frac{i\pi w}{L})}\right) \tag{51}$$

which were evaluated using 100 non-zero terms in the series.

A finite element mesh of 30x10 elements was used in the analyses, which were performed adopting 4, 8 and 9 node elements. The distortion effects were evaluated by applying two distortion patterns to the set of 4 elements highlighted in Fig.4. These patterns are shown in Fig. 5 particularized for the 9 nodes element. Extension to 4 and 8 node elements is straightforward.

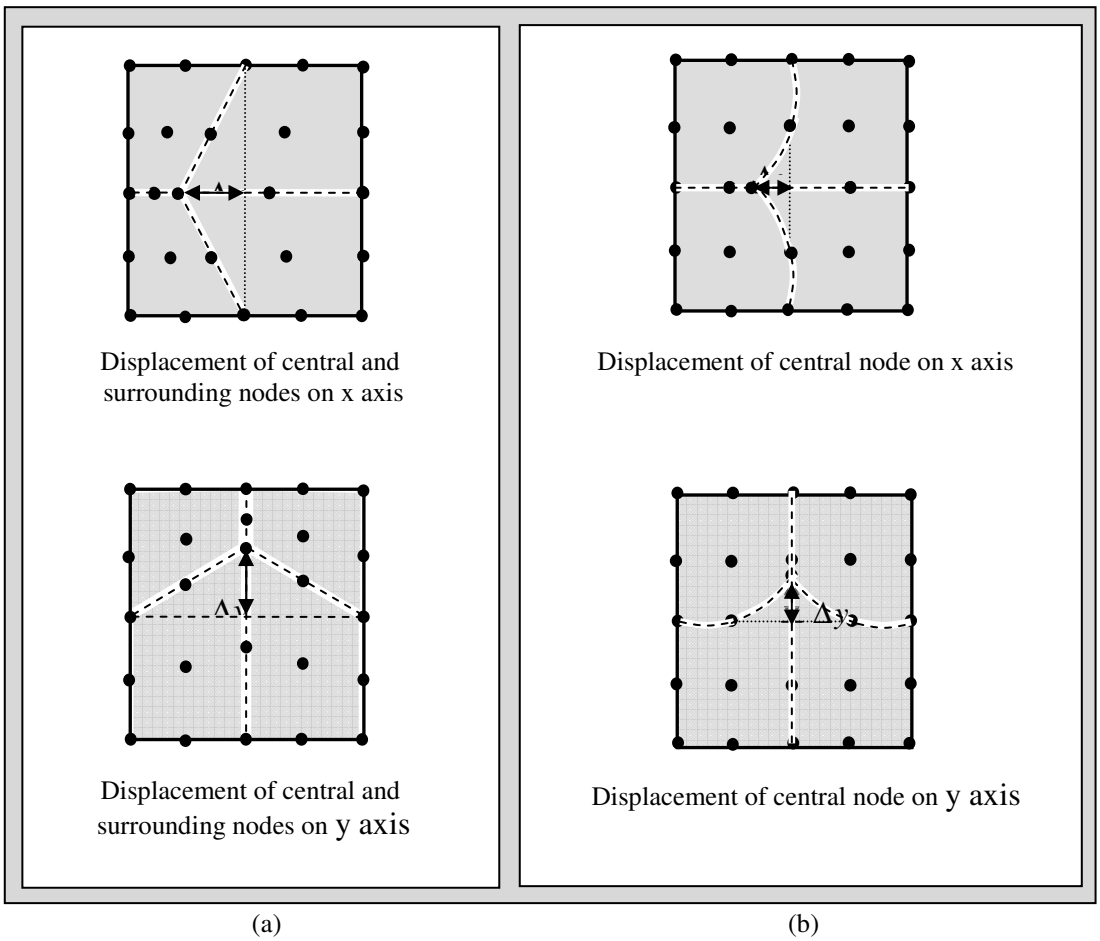

Figure 5. Distortion patterns for the 9 node element.

In the first pattern, Fig. 5(a), the node located at the center of the 4 elements set is simultaneously displaced horizontally and vertically and all the surrounding nodes keep their parametric positions, i.e. midside nodes are reallocated to stay at the midside. This is the situation that generally occurs when unstructured mesh generators are employed. In the

second pattern, Fig. 5(b), a more aggressive distortion pattern is imposed: the node at the center of the set is displaced and all the surrounding nodes keep their original positions. When large deformations occur or shape optimization is performed, the nodes can be subject to arbitrary displacements (not maintaining parametric positions) and severe distortion conditions like the ones simulated by this pattern can take place.

The distortion error is measured by

$$\|e\|_{nodal} = \left\|(q_{D,EF} - q_{D,ANALIT}) - (q_{ND,EF} - q_{ND,ANALIT})\right\|_{L2} \tag{52}$$

where $\|e\|_{nodal}$ is the L_2 norm measured at the central node, $q_{ND,EF}$ is the finite element flux vector evaluated in the undistorted mesh, $q_{ND,ANALIT}$ is the analytical flux vector evaluated in the undistorted mesh location, $q_{D,EF}$ is the finite element flux vector evaluated in the distorted mesh and $q_{D,ANALIT}$ is the analytical flux vector evaluated in the distorted mesh location. The flux nodal error at the undistorted condition was removed in order to place all the distortion graphs at the same origin. The graphs displaying the error levels for the distortions are shown in Figs. 6-7 for 4 node elements, Figs. 8-11 for 8 node elements and Figs. 12-15 for 9 node elements. Table 1 shows the heat flux error at the central node in the undistorted 4 node element mesh for all recovery methods. Table 2 shows the same information for undistorted 8 and 9 node element mesh.

Figs. 6-7 show that the SPRE and temperature patch schemes are clearly superior to the other schemes. In 4 node elements, evidently there is no difference between both distortion patterns proposed (there are no midside nodes).

In Figs. 8-9 it is clear that, when there is no relocation of the surrounding nodes, the error level can become very high with a relatively low distortion. This is expected, since as the displaced node approaches the midside one, the Jacobian becomes singular. However, SPRE and temperature patch schemes provide errors similar to the ones reported for 4 node elements, which are large but "controlled".

When relocation is applied to surrounding nodes, Figs. 10-11 show that 8 node elements provide errors one order of magnitude lower than without relocation and larger distortions can take place. Note that SPR and temperature patch recovery schemes are always better when compared to the other approaches. The same qualitative behavior is observed when 9 node elements are used, as depicted in Figs. 12-15.

nodes	D	E	S	PD6	PD8	PD9	SPRE	SPRE4
4	2.04E-03	4.61E-04	8.26E-04	1.10E-03	1.55E-03	1.62E-03	9.46E-04	2.88E-04

Table 1. Flux error of undistorted meshs for 4 nodes element.

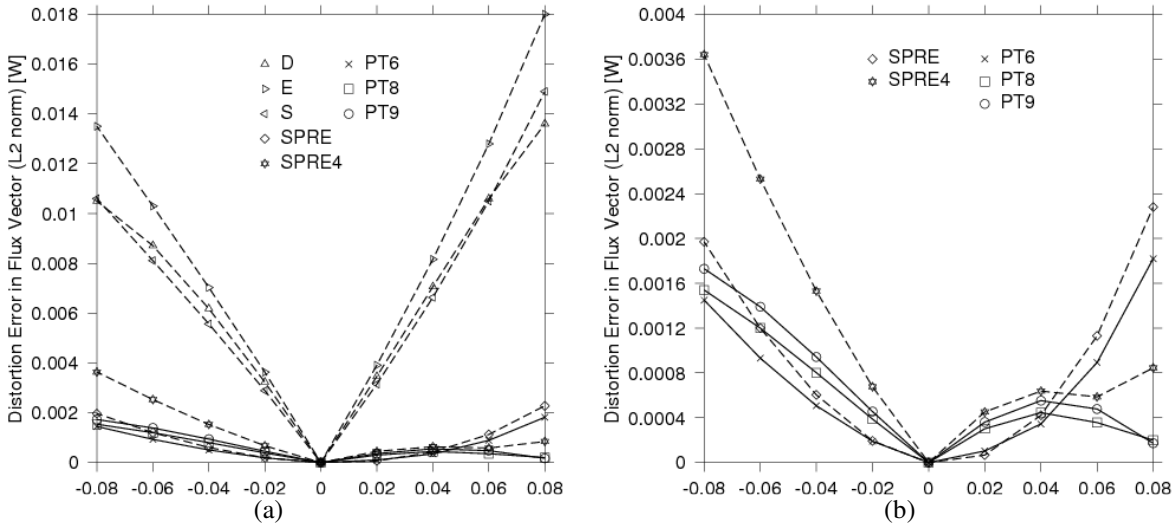

Figure 6. (a) Distortion flux error (L_2 norm) for 4 node element mesh under central node displacement on *x* direction. (b) Detail.

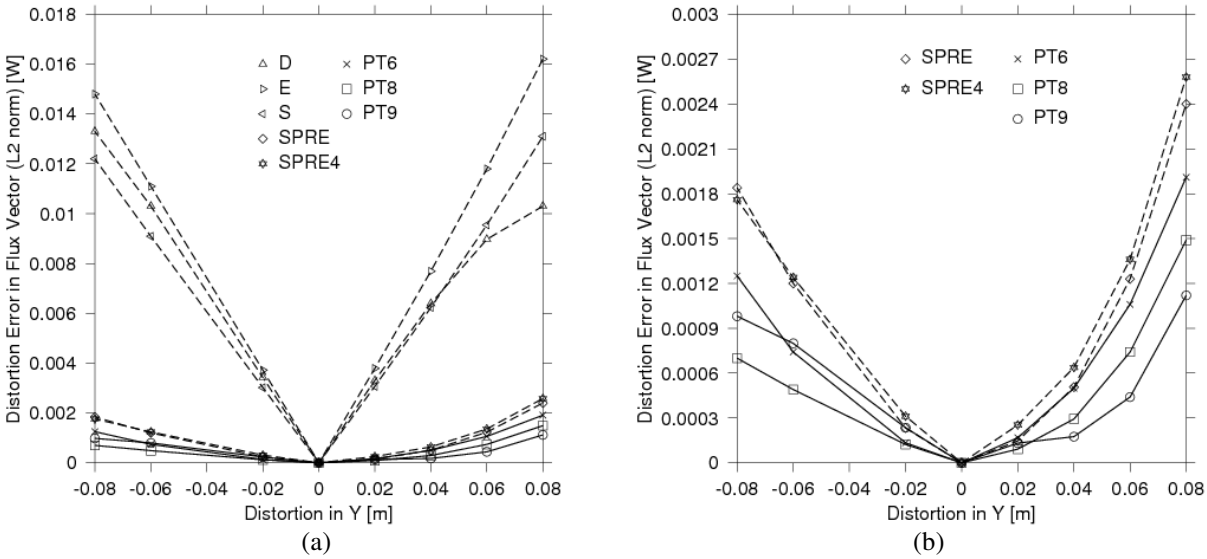

Figure 7. (a) Distortion flux error (L_2 norm) on 4 nodes element mesh under central node displacement on *y* direction. (b) Detail.

nodes	D	E	S	PD13	PD15	PD16	SPRE6	SPRE8	SPRE9
8	6.30E-04	1.76E-05	6.28E-04	1.34E-04	7.79E-05	8.00E-05	1.99E-04	1.87E-04	1.45E-04
9	6.34E-04	1.77E-05	6.28E-04	1.35E-04	7.80E-05	8.05E-05	1.99E-04	1.87E-04	1.45E-04

Table 2. Flux error of undistorted meshes for 8 and 9 nodes element

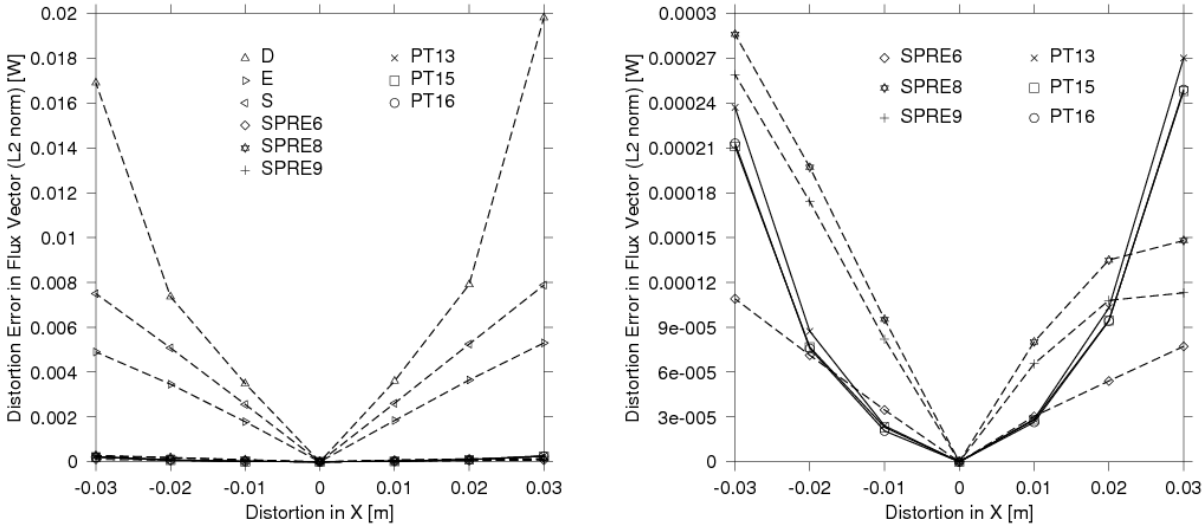

Figure 8. (a) Distortion flux error (L_2 norm) on 8 nodes element mesh under central node displacement on *x* direction. (b) Detail.

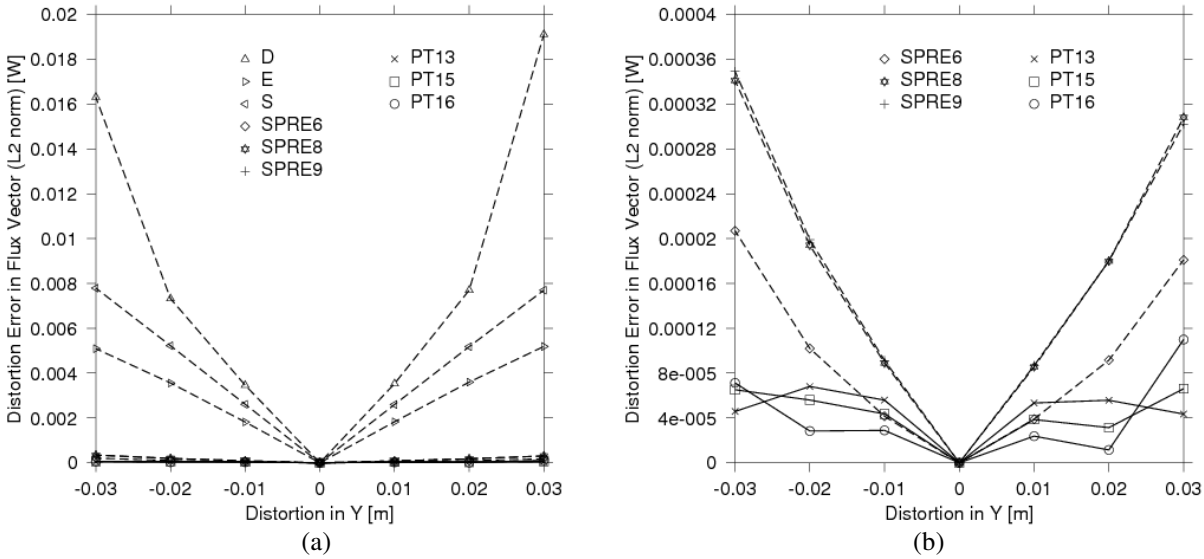

Figure 9. (a) Distortion flux error (L_2 norm) on 8 nodes element mesh under central node displacement on *y* direction. (b) Detail.

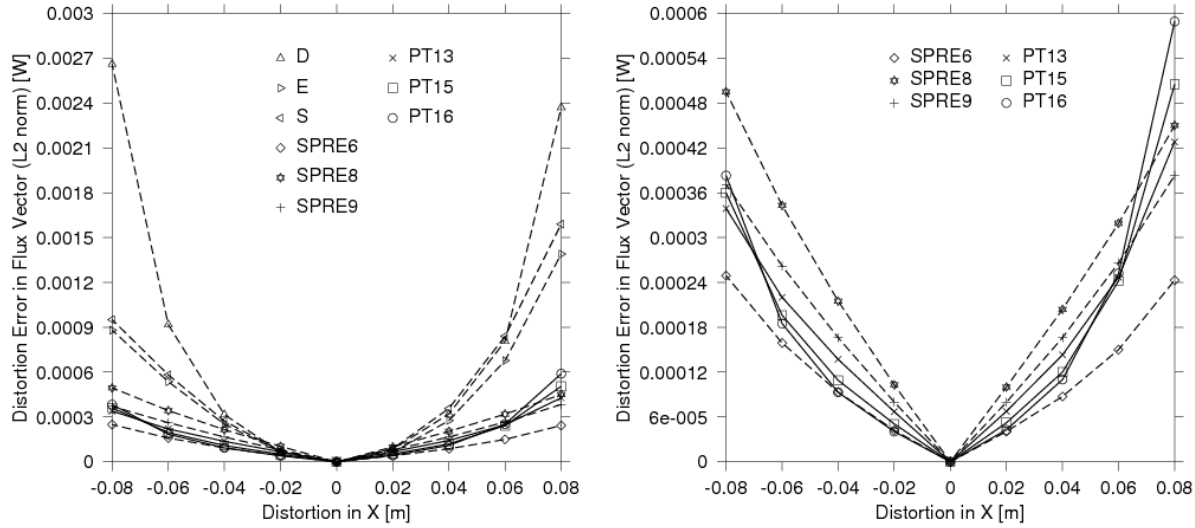

Figure 10. (a) Distortion flux error (L_2 norm) on 8 nodes element mesh under central and surrounding nodes displacement on *x* direction. (b) Detail.

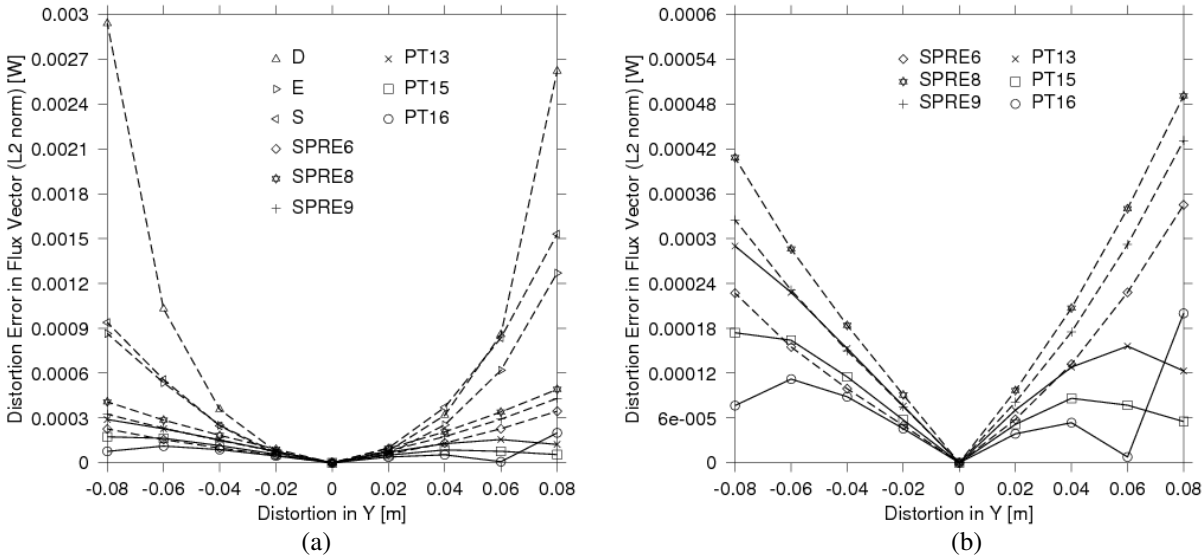

Figure 11. (a) Distortion flux error (L_2 norm) on 8 nodes element mesh under central and surrounding nodes displacement on *y* direction. (b) Detail.

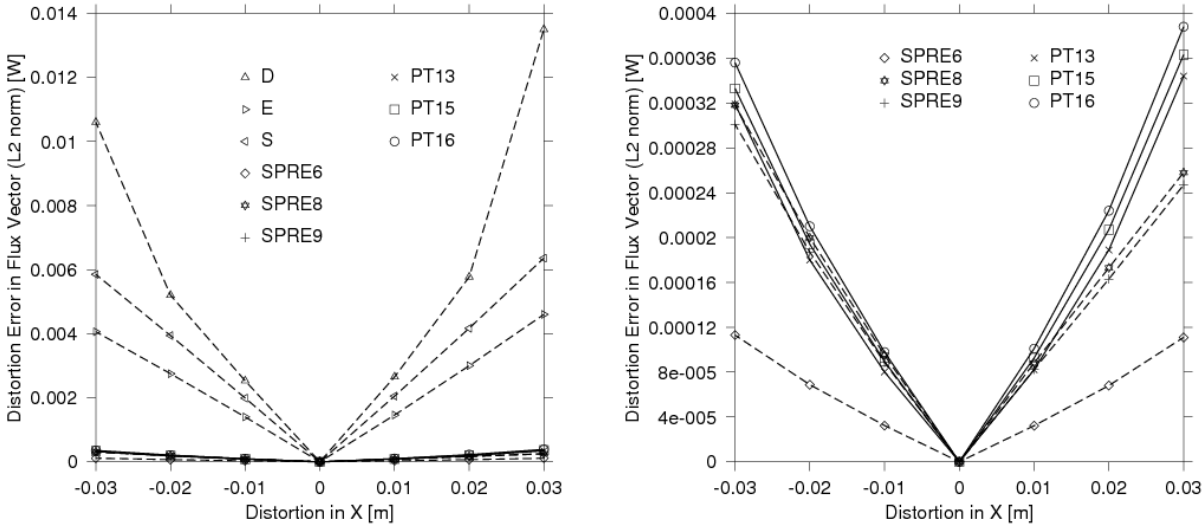

(a) (b)

Figure 12. (a) Distortion flux error (L_2 norm) on 9 nodes element mesh under central node displacement on *x* direction. (b) Detail.

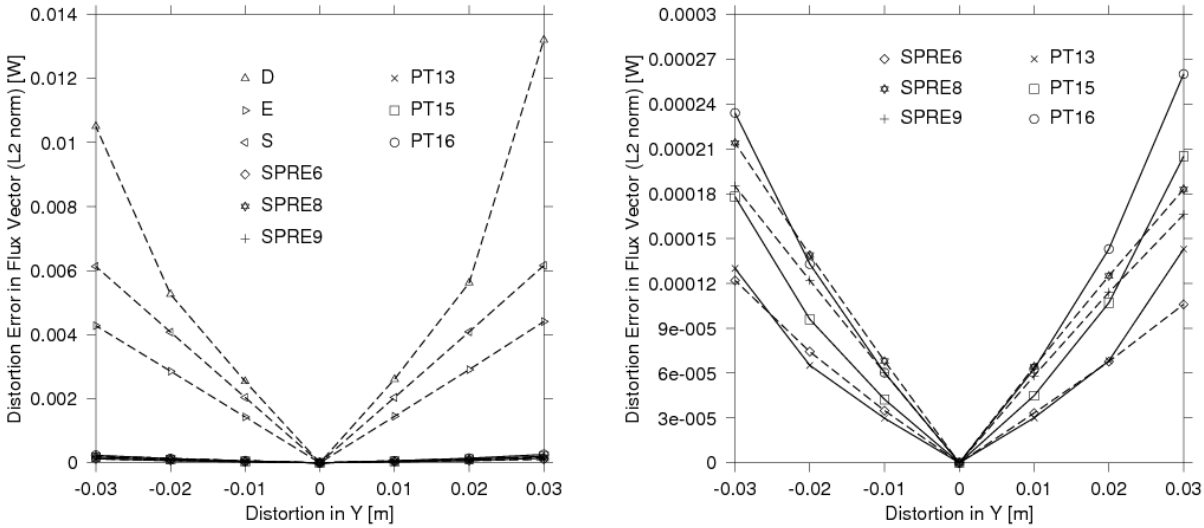

(a) (b)

Figure 13. (a) Distortion flux error (L_2 norm) on 9 nodes element mesh under central node displacement on *y* direction. (b) Detail.

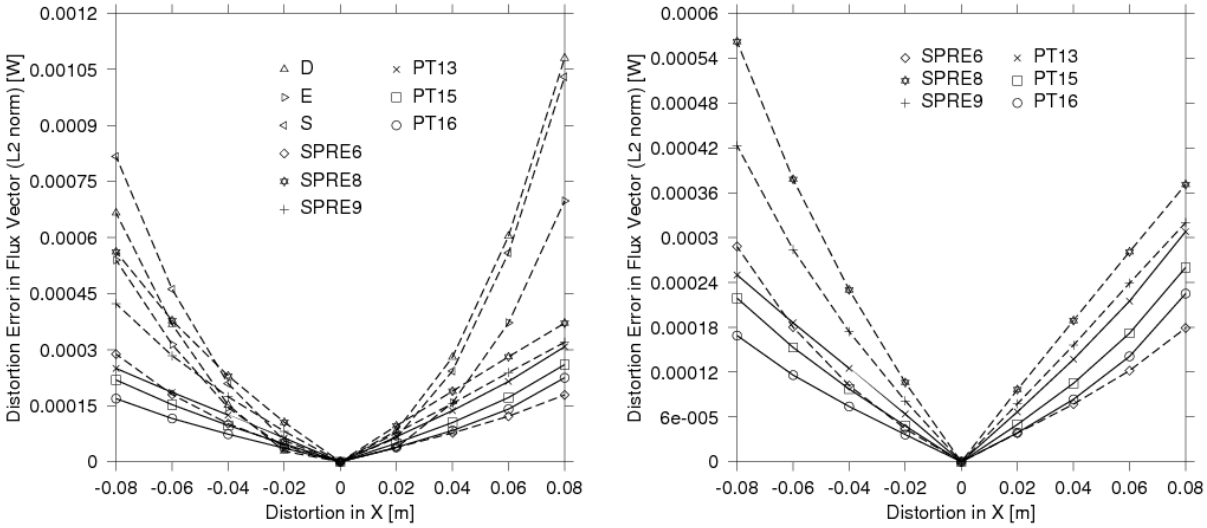

Figure 14. (a) Distortion flux error (L_2 norm) on 9 nodes element mesh under central and surrounding nodes displacement on *x* direction. (b) Detail.

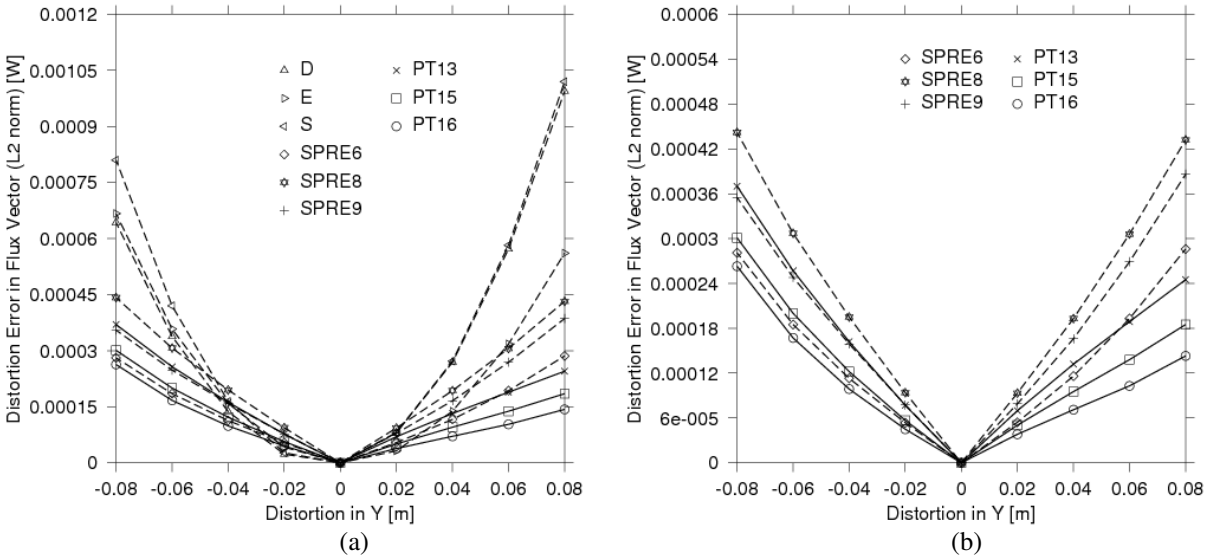

Figure 15. (a) Distortion flux error (L_2 norm) on 9 nodes element mesh under central and surrounding nodes displacement on *y* direction. (b) Detail.

5.2 Convergence rate in a smooth problem

In order to evaluate the convergence rate of the global heat flux error (L_2 norm), the Temperature Patch flux recovery scheme (PT) is compared to different flux post-processing schemes: (D, E, S and SPRE). A smooth heat transfer problem (no singularities) with known analytical solution is chosen, which consists of a 2D square plate, with 20x20 m^2 area and unit width, subjected to prescribed temperature in all boundaries, as shown in Fig. 16. The material has isotropic properties and the thermal conductivity is $k = 1$ W/mK .

The prescribed temperatures at the right, left and bottom surfaces are 0 ^{o}C. The upper boundary surface is subjected to $T = \sin(\pi x/L)$ in order to avoid singularity points at the right and left top corners.

For the numerical solution, square quadrilateral 4 node and 9 node element meshes are used, with element size *h* ranging from $h_0 = 10$ m to $h_6 = 0.15625$ m according to

$$h_{i+1} = h_i/2 \tag{53}$$

where $h_0 = 10$ m and *i*=1 to 6

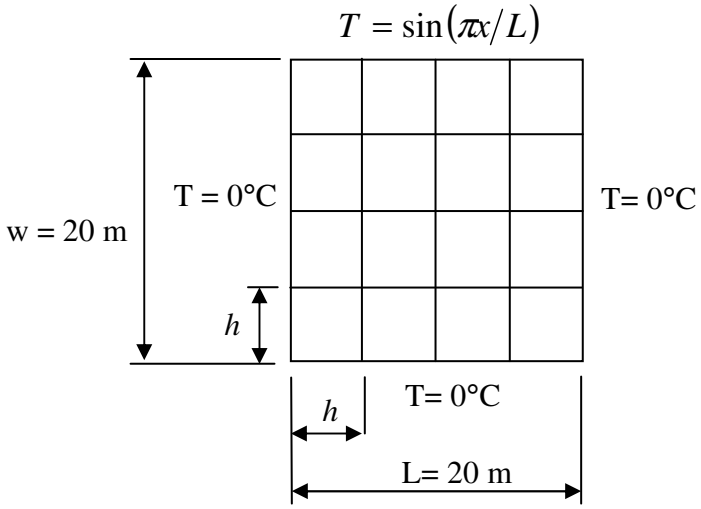

Figure 16. 2D plate with prescribed temperature boundary conditions.

The error in flux vector (L_2 norm) is calculated according to

$$\|e\|_{L_2} = \|q_{EF} - q_{analit}\|_{L_2} = \left[\int_V (q_{EF} - q_{analit})^T (q_{EF} - q_{analit}) dV\right]^{1/2} \tag{54}$$

where q_{EF} is the recovered nodal heat flux and q_{ANALIT} is the analytical heat solution as

$$q_x = -k\frac{\pi \sinh\left(\frac{\pi y}{L}\right)\cos\left(\frac{\pi x}{L}\right)}{L\sinh\left(\frac{\pi w}{L}\right)} \qquad q_y = -k\frac{\pi \cosh\left(\frac{\pi y}{L}\right)\sin\left(\frac{\pi x}{L}\right)}{L\sinh\left(\frac{\pi w}{L}\right)} \tag{55-56}$$

The convergence rate of each flux recovery method is given by the slope of the curve of the global heat flux error versus the element size *h,* both in log scale. The convergence rate results for the 4 node elements are displayed in Fig. 17(a) and Table 3, whereas results for 9 node elements are presented in Fig.17(b) and Table 4.

Note that for both element types the error level for all flux recovery schemes decreases with mesh refinement. Also in both element cases, the patch recovery procedures (PT's and SPRE's) present smaller errors and higher convergence rate for the heat flux errors (L_2 norm) than the Direct, Smoothed and Extrapolated Methods (D, S, E).

For 4 node element meshes, the patch procedures (SPRE's and PT's) present a higher order of convergence rate than D, E, S methods that have first order. For 9 node element meshes

this behavior is more pronounced and show cubic order for SPRE and PT patch procedures and quadratic order for D, E and S techniques.

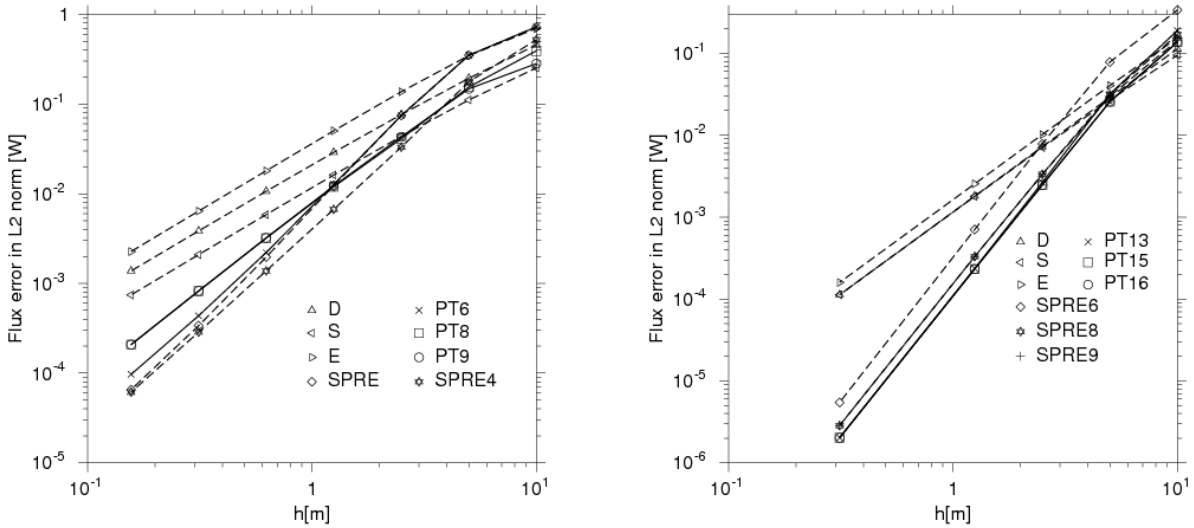

Figure 17. Convergence rate of the flux error measured in L_2 norm: (a) 4 node element and (b) 9 node element.

D	E	S	SPRE	SPRE+	PT6	PT8	PT9
1.4023	1.401	1.4134	2.3417	2.2241	2.2488	1.8368	1.7833

Table 3. Convergence rate of the flux error in the L_2 norm for 4 node element.

D	E	S	SPRE	SPRE8	SPRE9	PT13	PT15	PT16
1.9966	1.987	1.9512	3.2566	3.2172	3.1753	3.3593	3.2639	3.2639

Table 4. Convergence rate of the flux error in the L_2 norm for 9 node element.

5.3 Assessment of the flux recovery on the boundary

This example discusses the quality of the heat flux on the boundary provided by the recovery techniques described in Sections 3 and 4. A heat transfer problem with prescribed heat flux is analyzed. The proposed example consists of a 2D flat plate with 10x10 m^2 area and unit width, subjected to prescribed temperature in three surfaces and prescribed heat flux on the top boundary, as presented in Fig. 18. The material has isotropic properties and the thermal conductivity is k = 1.0 W/mK. The prescribed temperatures at the right, left and bottom surfaces are 0.0 ^{o}C. The top boundary is subjected to a heat flux q_y = 10 *W*. For the numerical solution, quadrilateral 4, 8 and 9 node element meshes are used with element size h ranging from h = 0.5 m to h = 1.0 m.

The accuracy of the each heat flux recovery method is evaluated by the relative error of the numerical result compared to the heat flux prescribed in the *y* direction, as

$$e_y = \left(\frac{q_{num_y} - q_{prescr_y}}{q_{prescr\,y}} \right) 100 \quad [\%] \tag{57}$$

where e_y is the relative error of heat flux in the *y* direction, $q_{num\,y}$ is the numerical nodal

result obtained by each flux recovery method and $q_{prescr\ y}$ is the prescribed heat flux. Both flux quantities are considered in the *y* direction at the top surface.

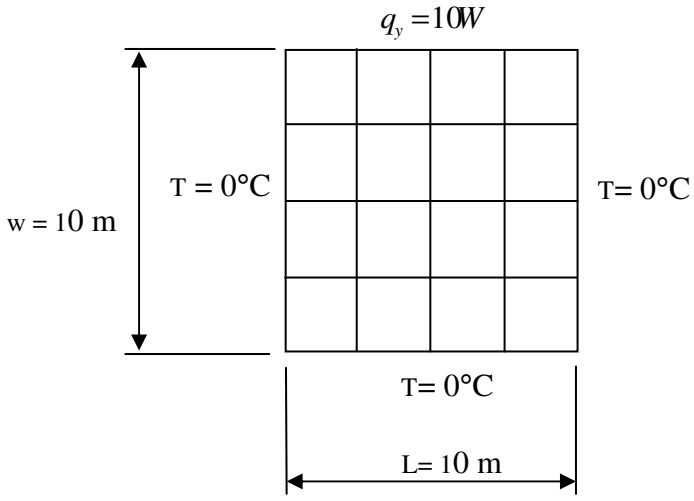

Figure 18. 2D body under Temperature and Flux Field

The relative error results for the 4 node elements are presented in Figs. 19-20, for the 8 node elements are displayed in Figs. 20-21, and for the 9 node elements the results are shown in Figs. 22-23.

Note that the error level of all flux recovery schemes decreases drastically when the number of nodes per element increases and also with mesh refinement. At the corners the result for all methods is very poor and must not be considered. Observation of the results in the interval between 1 to 9 [m] on the upper edge leads to the considerations described in the following paragraphs.

For the 4 nodes mesh in Figs 19-20, the general results of a 400 elements mesh are better then the results for 100 elements mesh. For both mesh sizes the patch procedures (superconvergent SPRE's and Temperature Patch PT's) have similar results and clearly superior than the Direct, Smoothed and Extrapolated Methods (D, S, E) both at the corners and near the center of upper edge.

As shown in Figs. 21-24, the results for 8 and 9 node elements present similar behavior as the 4 nodes mesh with respect to mesh size and total number of nodes. The Temperature Patch method shows similar results as the superconvergent and D, E, S methods.

In special, the Temperature Patch method with 8 terms (PT8) applied to a 4 node finite element mesh and the Temperature Patch with 15 terms (PT15) applied to a 8 or 9 node element show, for the present study case, better accuracy with respect to the level (not taking into account peak values) of relative error in heat flux at the upper edge.

In all cases the Temperature Patch method shows similar results compared to superconvergent methods and, especially for 4 nodes element, they are superior than D, E, S methods. For 8 and 9 element nodes with coarse meshes, the D, E, S methods improve their performance but are still far less accurate than patch procedures. For 8 and 9 element nodes with refined meshes, the D, E and S methods increase accuracy and present results comparable to patch procedures.

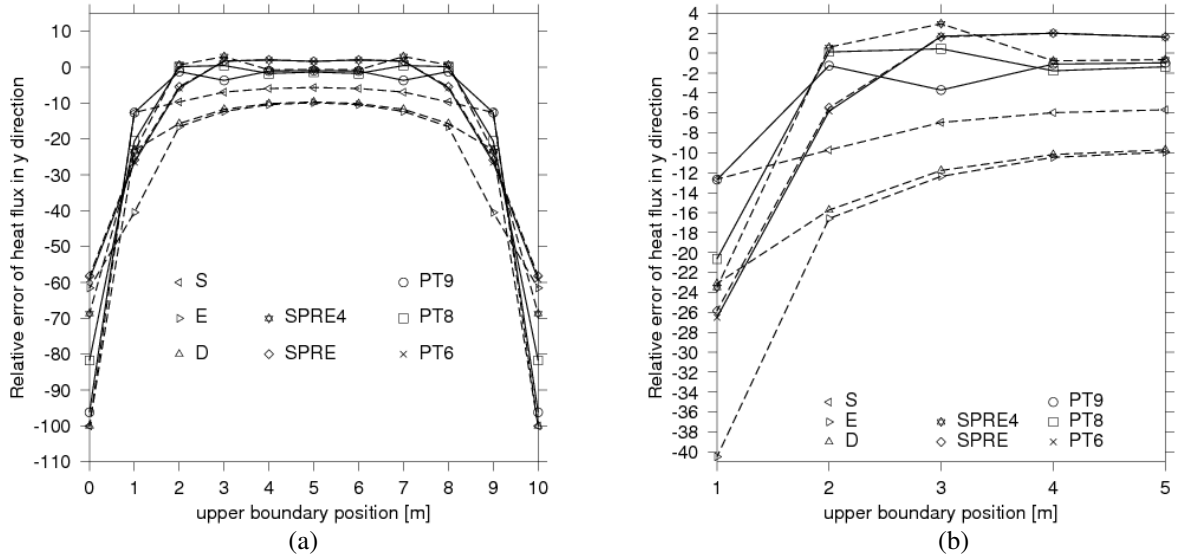

(a) (b)

Figure 19. (a) Assessment of flux recovery methods in *y* direction for quadrilateral 4 nodes element, mesh 10x10. (b) Detail.

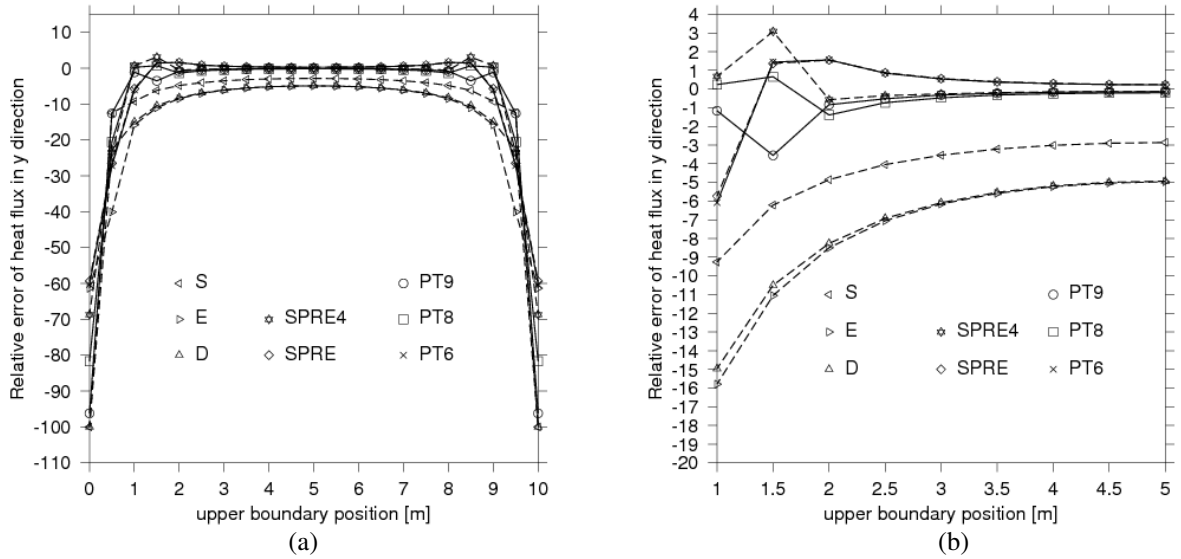

(a) (b)

Figure 20. (a) Assessment of flux recovery methods in *y* direction for quadrilateral 4 nodes element, mesh 20x20. (b) Detail.

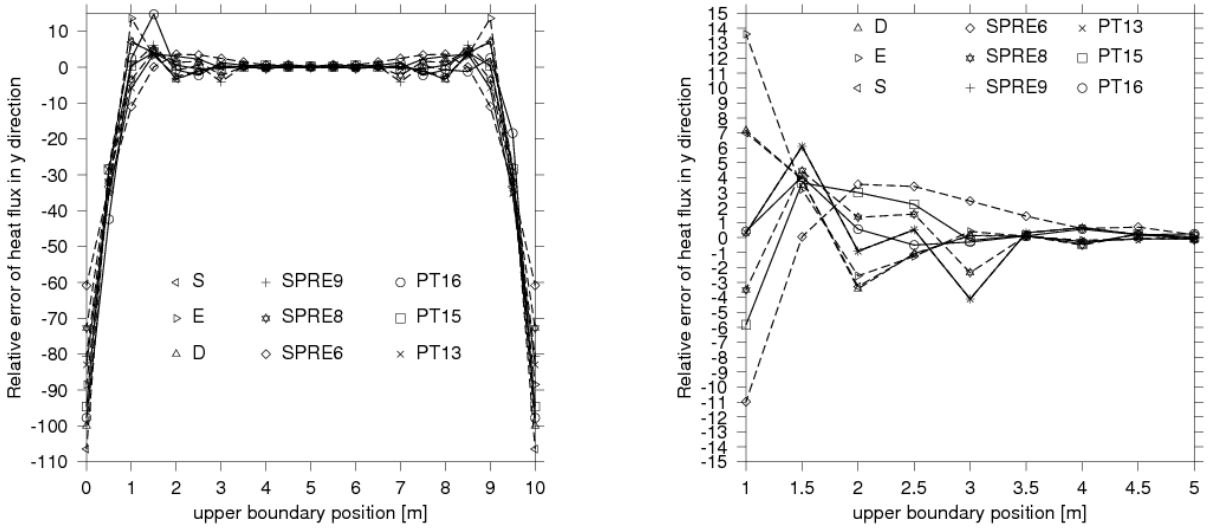

(a) (b)

Figure 21. (a) Assessment of flux recovery methods in *y* direction for quadrilateral 8 nodes element, mesh 10x10. (b) Detail.

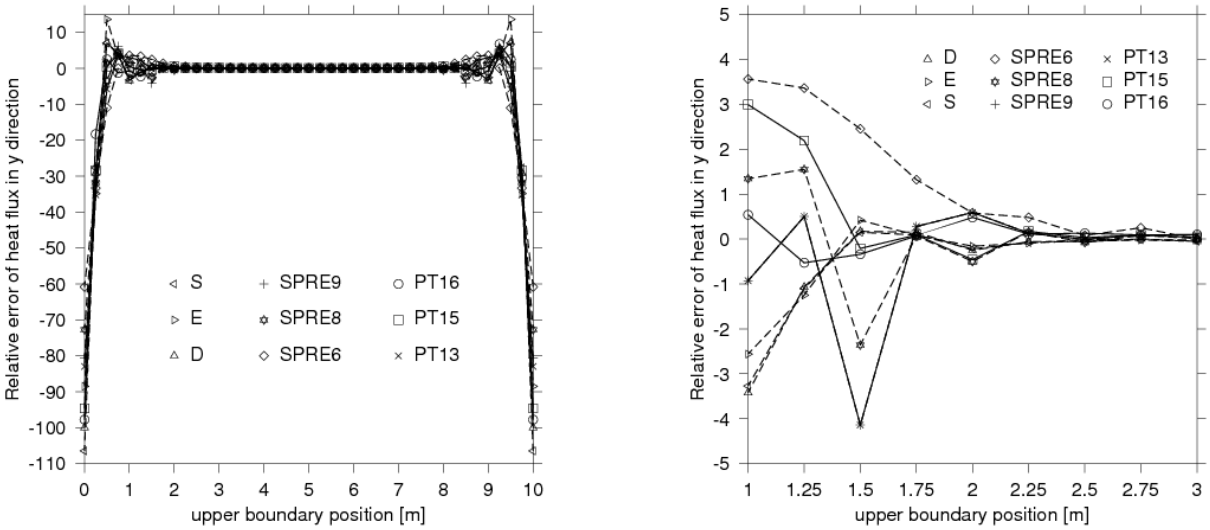

(a) (b)

Figure 22. (a) Assessment of flux recovery methods in *y* direction for quadrilateral 8 nodes element, mesh 20x20. (b) Detail.

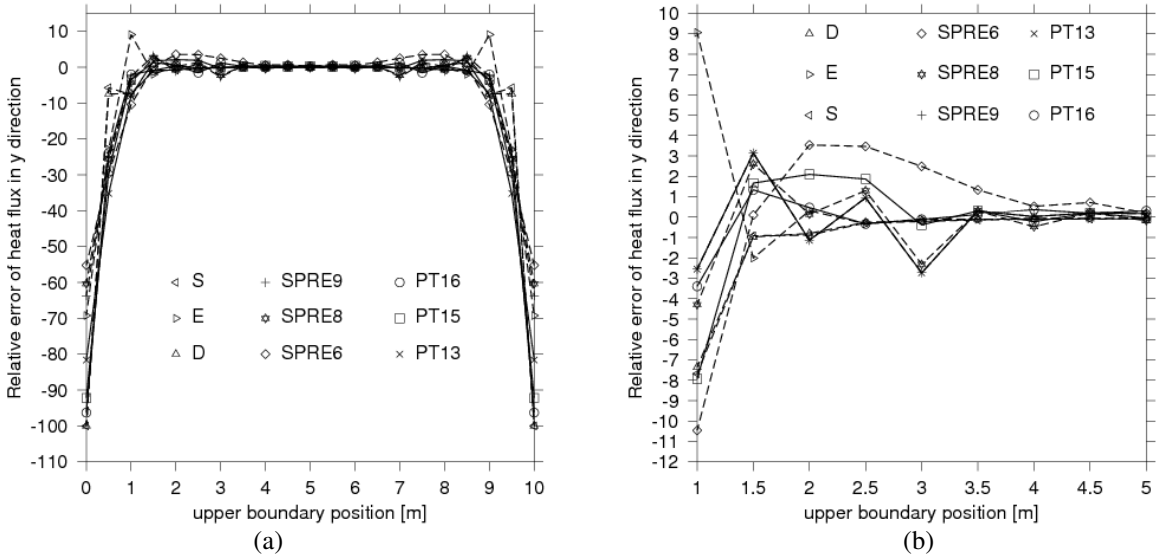

(a) (b)

Figure 23. (a) Assessment of flux recovery methods in *y* direction for quadrilateral 9 nodes element, mesh 10x10. (b) Detail

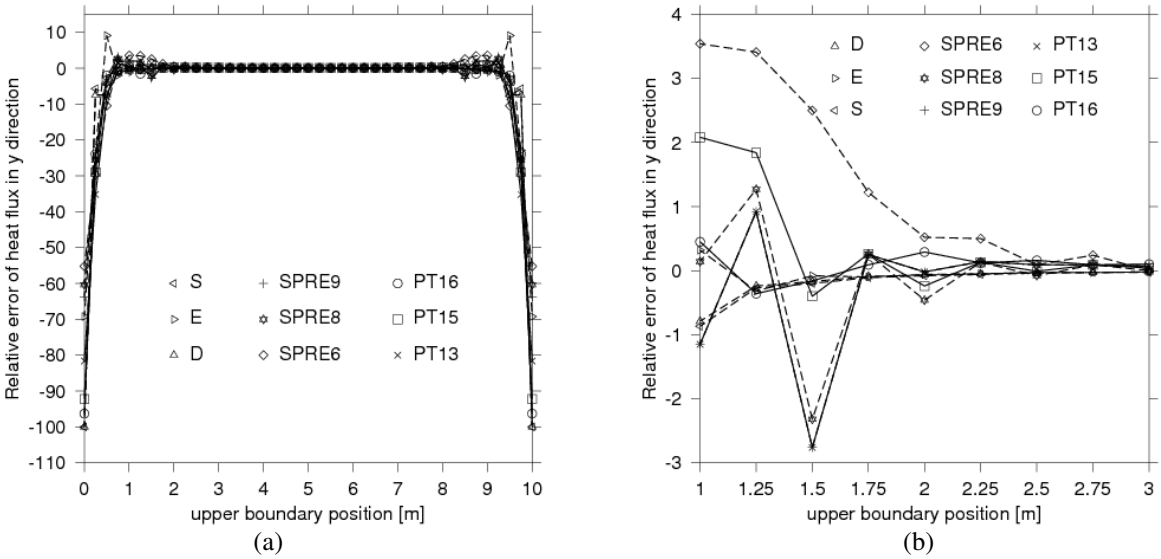

(a) (b)

Figure 24. (a) Assessment of flux recovery methods in *y* direction for quadrilateral 9 nodes element, mesh 20x20. (b) Detail.

6 CONCLUSIONS

The proposed method for heat flux recovery based on Temperature Patch (PT) presents similar results when compared to the superconvergent method with an advantage on computational time reduction. The recovery scheme based on temperature patches is superior to Direct, Smoothed and Extrapolated Methods in all points analyzed regarding mesh distortion, convergence rate and accuracy of results.

REFERENCES

Akin, J. E., Finite Element Analysis with Error Estimators: An Introduction to the FEM and Adaptive Error Analysis for Engineering Students, Butterworth-Heinemann, 2005.

Barlow, J., Optimal stress locations infinite element models. *International Journal for Numerical Methods in Engineering*, 10:243-251, 1976.

Boroomand, B. and Zienkiewicz, O. C., Recovery by equilibrium in patches (REP). *International Journal for Numerical Methods in Engineering*, 40:137-164, 1997.

Cook, R.D., Malkus, D.S., Plesha, M.E., *Concepts and Applications of Finite Element Analysis*, John Wiley & Sons, 3rd. edition, 1989.

Hinton, E. and Campbell, J. S., Local and global smoothing of discontinuous finite element functions using a least squares method. *International Journal for Numerical Methods in Engineering*, 8:461-480, 1974.

Kreith, F. and Bohn, M. S., Principles of Heat Transfer, CL-Engineering, 6th edition, 2010.

Wildemann, F. and Muñoz-Rojas, P. A., Stress recovery techniques applied to plane elasticity and solids of revolution. In *Iberian Latin American Conference on Computational Methods in Engineering*, Guarapari, ES, Brazil, 2005.

Zienkiewicz, O. C. & Zhu, J. Z. The superconvergent patch recovery and a posteriori error estimates. Part 1: The recovery technique. *International Journal for Numerical Methods in Engineering,* 33:1331-1364, 1992.